Available online at www.sciencedirect.com
ScienceDirect
International Journal of Solids and Structures 44 (2007) 6653–6677
INTERNATIONAL JOURNAL OF SOLIDS AND STRUCTURES
www.elsevier.com/locate/ijsolstr

The effect of path cut on Somigliana ring dislocation elastic fields

Robert J.H. Paynter *, David A. Hills, Alexander M. Korsunsky

Department of Engineering Science, University of Oxford, Parks Road, Oxford OX1 3PJ, United Kingdom

Received 17 June 2006; received in revised form 6 February 2007
Available online 7 March 2007

Abstract

In this paper we look at ring dislocations (circular loops) in an infinite isotropic full-space. The dislocation direction is either axial or radial. Unlike dislocations in plane analysis the path cut has a significant effect on the elastic fields. Solutions for the dislocations are given for a variety of path cuts with closed form expressions for the displacement and stress fields. When considered alone these dislocations do not obey Frank's rule; these anomalies and other fundamental properties are discussed.

Keywords: Dislocations; Somigliana; Axisymmetric

1. Introduction

Dislocations were hypothesised at the end of the 19th century and subsequently (1930s) proposed to explain the difference between the Frenkel calculation for the theoretical strength of a crystalline solid, and measured values. Their existence was, of course, subsequently verified experimentally: dislocations in crystalline solids are of the Volterra kind (Christian and Crocker, 1980), and, in solid mechanics terms, may be formed by taking a cut along a surface from the dislocation line to infinity, displacing the two surfaces everywhere by a constant amount, the Burgers vector, adding or removing material as necessary, and glueing the cut surface back together. Volterra dislocations have, amongst other properties, the features that the Burgers vector is constant along the path cut and that the state of stress induced is *independent* of the location of the surfaces (i.e. it is path-cut independent). The stress induced by the procedure varies like $1/r$, where r is a coordinate measured from the dislocation line and orthogonal to it, and hence has no long-range resultant. This last property, in particular, makes dislocations attractive in another field entirely: they can be used as strain nuclei to perturb the state of stress in a solid in a controlled way, possibly to model plastic flow (Blomerus and Hills, 1998), or to solve crack problems. The latter procedure was developed extensively by Dundurs, Keer, Comninou and others in the 1970s, and some of the techniques were summarised by Hills et al. (1996). In this paper we wish to

* Corresponding author. Tel.: +44 1865 283489.
E-mail address: robert.paynter@eng.ox.ac.uk (R.J.H. Paynter).

0020-7683/$ - see front matter © 2007 Elsevier Ltd. All rights reserved.
doi:10.1016/j.ijsolstr.2007.03.001

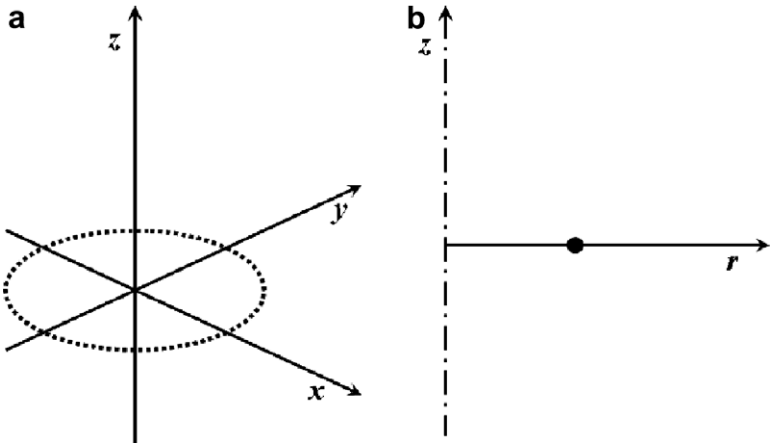

Fig. 1. Ring dislocation and axes.

examine one geometry of a dislocation loop – when it is a circle – and to examine, in particular, the properties of the solution when the Volterra assumptions do not hold.

Fig. 1(a) shows an axis set present in an infinite space, with the dislocation loop, of radius a, lying in the $x-y$ plane. Two types of Volterra type edge dislocation can be identified: the climb or prismatic loop, when the Burgers vector lies in the z-direction, and the glide loop when it lies in the $x-y$ plane. The literature includes solutions for climb loops in an infinite space (Korsunsky, 1996a; Kroupa, 1960; Salamon and Comninou, 1979) and a half-space (Korsunsky, 1996b; Salamon and Dundurs, 1971). The glide loop is less comprehensively covered, but solutions for an infinite and half spaces are given for example in Salamon and Dundurs (1977). These solutions are of value in studying crystalline defects, but the glide loop is of very limited value as a strain nucleus, as it is not inherently axisymmetric. A much more useful strategy for axisymmetric crack problems is to develop a dislocation solution family based on the cylindrical coordinate set shown in Fig. 1(b). Clearly, the prismatic loop (Burgers vector b_z) is equally valuable here, and the 'twist loop', in which the Burgers vector of the dislocation is tangential to the dislocation line is very useful for torsional problems. In the latter case the Burgers vector varies in direction around the loop but there was little difficulty in developing a solution for both an infinite space and a half-space (Sackfield et al., 2002). The remaining dislocation solution needed is one for a radial Burgers vector (b_r). There are existing solutions by Korsunsky (1996a) and by Demir et al. (1992), but these make intrinsic assumptions about the path cuts used to form the dislocation, and these may or may not be consistent with the intended application. Because generalised Somigliana dislocations are being considered the state of stress induced *is* dependent on the path cut, and, as will be shown, there are further complications in their exploitation as strain nuclei. The object in the present paper is to provide a definitive solution for both kinds of axisymmetric ring dislocations, in an infinite space. Although there are pre-existing solutions, listed above, none of them has sought to emphasize the difficulties which arise when analysing the radial dislocation, and this is particularly important when dislocations are to be employed as strain kernels.

2. Dislocation definitions

A plane edge dislocation may be formed, in solid mechanics terms, either by making a cut along the glide plane and displacing the adjacent surfaces in shear by the Burgers vector, or by making a cut from the core perpendicular to the glide plane, and inserting a thin sheet, of the same material, of thickness equal to the Burgers vector. The stress field induced by each is identical, and so is the component of the displacement field perpendicular to the Burgers vector, to within an arbitrary constant. However the component of displacement parallel with the Burgers vector suffers a jump when the path cut is crossed, and hence differences do arise. When dislocations are used to model cracks the path cuts should be arranged to lie along the line of the crack,

so that the cumulative Burgers vectors of the dislocations represent the crack opening displacement and crack shear displacement.

In three dimensions the cuts are surfaces and indeed, as we are concerned with an axisymmetric geometry, they lie on conic surfaces. In our treatment we deal with three cut surfaces: (a) a plane, perpendicular to the axis with finite radius – a disc, (b) the same plane but with the cut everywhere external to the disc and (c) a cylindrical surface extending to infinity in one direction.

Our dislocations derive from the positioning of the cut surfaces and the displacement discontinuities at those surfaces. The dislocations be considered as distributions of surface dislocation densities, as used by Hurtado and Weertman (1995), however in our analysis we consider the integration, thus displacement discontinuities.

All dislocations must satisfy certain boundary conditions: the stresses must, of course, satisfy the field equations, and must be continuous everywhere save at the branch cut: there, the direct stress parallel with the surface of the cut may be discontinuous, but the traction components must be continuous. The displacement component orthogonal to the Burgers vector must also be continuous across the branch cut.

2.1. Boundary conditions

Consider, now, three ways of forming an axisymmetric *radial* generalised dislocation, of Burgers vector b_r, Fig. 2. In Fig. 2(a) a cut is made on the $z = 0$ plane, from the circle $r = a$ to infinity, and the upper surface displaced outwards by b_r relative to the lower surface, just exterior to the disc. In order to ensure that the stresses vanish for large values of r the relative slip displacement is required to decrease in inverse proportion to the radius, before gluing the surfaces back together, and hence we may formally write

$$\lim_{\epsilon\to 0}(u_r(r > a, -\epsilon) - u_r(r > a, +\epsilon)) = \frac{a}{r} b_r^{\mathrm{o}} \tag{1}$$

where we have added a superscript o to denote a cut on the *outside* of the disc defining the plane of the dislocation. This forms a radial *glide* dislocation, and because the path cut was made in the plane of the loop, is appropriate (together with a prismatic dislocation) when modelling a disc-crack.

It is possible to form the same dislocation by making the cut *within* the disc $r < a$, and here, because the displacement must fall to zero on the centre-line ($r = 0$), a linearly increasing radial displacement with r would be needed, and hence the displacement-discontinuity definition is

$$\lim_{\epsilon\to 0}(u_r(r < a, +\epsilon) - u_r(r < a, -\epsilon)) = \frac{r}{a} b_r^{\mathrm{i}} \tag{2}$$

where we have added the superscript i to denote that the slip displacement is imposed on the *inside* of the disc defining the plane of the dislocation.

A dislocation with the same Burgers vector could also be made by inserting material, as shown in Fig. 2(b). Here a tubular cut is made from the plane of the dislocation, of radius equal to that of the dislocation loop, a, in the positive z direction, to infinity, a thin tube of material, of thickness b_r is inserted, and the material bonded back together, giving a radial *climb* dislocation. The definition of the dislocation is therefore

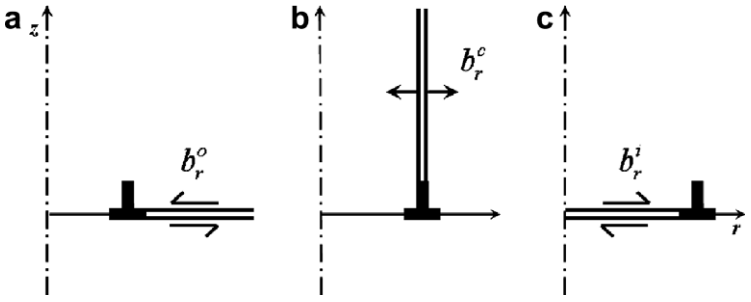

Fig. 2. Path cut surfaces.

$$\lim_{\epsilon\to 0}(u_r(a+\epsilon, z>0) - u_r(a-\epsilon, z>0)) = b_r^{\mathrm{c}} \tag{3}$$

where the superscript c denotes a *cylindrical* path cut. In this form the dislocation is appropriate for modelling debonding of fibres in an elastically similar matrix, for example. It is clear that, for the second kind of dislocation, there is a stress induced at large values of positive z, because this is very like the classical 'thick cylinder' problem. Korsunsky (1996a) noted this feature and the inherent asymmetry of the solution in z, and suggested ways of rendering the correct symmetry: we shall address this point in detail in due course.

It may be noted that the *prismatic* circular Volterra dislocation (having Burgers vector b_z) could also be formed in one of two ways: the most obvious is to make a cut over the disc $r < a \cap z = 0$ and to insert a thin disc material of Burgers vector b_z to give the displacement jump

$$\lim_{\epsilon\to 0}(u_z(r<a, +\epsilon) - u_z(r<a, -\epsilon)) = b_z^{\mathrm{i}} \tag{4}$$

Indeed, it would be possible to make the cut from $r = a$ to infinity, and to remove a thin sheet, also of thickness b_z, before gluing the surfaces back together, but as this is of extremely limited use this will not be pursued here: either would form a *climb* dislocation. But this is not the only option: an alternative strategy would be to make the cut along the cylinder $r = a$ and then to impose a shear direction displacement equal to the Burgers vector b_z

$$\lim_{\epsilon\to 0}(u_z(a+\epsilon, z>0) - u_z(a-\epsilon, z>0)) = b_z^{\mathrm{c}} \tag{5}$$

which is *glide* in character.

To summarise, there are two possible directions for the Burgers vector: axial (b_z) or radial (b_r), the former corresponding to a Volterra dislocation. There are three obvious choices of path cut which may be used to form each, and we denote these by superscripts: i, o, c (inner, outer, cylinder). We expect the state of stress induced by the prismatic dislocation to be path cut independent, as will the radial component of displacement, u_r. This dislocation also has the property that, remote from the dislocation line, the state of stress falls continuously to zero. These attributes are not, in general, true for the radial dislocation.

3. Papkovich–Neuber displacement potentials

The elastic solutions will all be presented in terms of Papkovich–Neuber potential functions. These have great utility because to find the displacements and stresses only requires differentiation of the potentials. A further reason for embarking on this approach is that a method exists that allows a ready extension of the potentials to a half space (or bonded, elastically dissimilar half spaces), and this will be dealt with in a sequel.

The Papkovich–Neuber potentials comprise a scalar quantity, ψ, and a vector quantity, $\boldsymbol{\phi}$, with components corresponding to each coordinate direction. The general form of the displacement–potential relations is

$$2\mu u_i = (\kappa+1)\phi_i - (x_j\phi_j + \psi)_{,i} \tag{6}$$

where the variable of partial differentiation is indicated by the subscript after the comma, $\kappa = 3 - 4\nu$, ν is the Poisson's ratio, and μ is the shear modulus. The solutions are not unique and it is found that one of the four components is not needed; in our case we choose to omit ϕ_r. A further simplification, is that $\phi_\theta = 0$, since there is no θ direction displacement. Then, simplifying the notation for the only remaining component $\phi \equiv \phi_z$, and noting that derivatives with respect to θ vanish we may write:

$$\begin{aligned} 2\mu u_r &= -z\phi_{,r} - \psi_{,r} \\ 2\mu u_z &= \kappa\phi - z\phi_{,z} - \psi_{,z} \\ 2\mu u_\theta &= 0 \end{aligned} \tag{7}$$

In cylindrical coordinates the expressions for the stress components are[1]

[1] The expression for $\sigma_{\theta\theta}$ has been derived *ab initio* and agrees with that given by Barber (2002). Both Korsunsky (1996a) and Salamon and Dundurs (1971) have fewer terms. The second expression for σ_{rr} is found using Laplace's equation, and results in less complex, differential operations with respect to r.

$$\begin{aligned}
\sigma_{rr} &= \frac{1}{2}(3-\kappa)\phi_{,z} - z\phi_{,rr} - \psi_{,rr} = \frac{1}{2}(3-\kappa)\phi_{,z} + z\phi_{,zz} + \frac{z}{r}\phi_{,r} + \psi_{,zz} + \frac{1}{r}\psi_{,r} \\
\sigma_{zz} &= \frac{1}{2}(\kappa+1)\phi_{,z} - z\phi_{,zz} - \psi_{,zz} \\
\sigma_{\theta\theta} &= \frac{1}{2}(3-\kappa)\phi_{,z} - \frac{z}{r}\phi_{,r} - \frac{1}{r}\psi_{,r} \\
\sigma_{rz} &= \frac{1}{2}(\kappa-1)\phi_{,r} - z\phi_{,rz} - \psi_{,rz}
\end{aligned} \tag{8}$$

4. Generalised Lipschitz–Hankel integrals

Lipschitz–Hankel integrals are heavily drawn upon in many of the papers to date relating to the solutions for circular dislocations (Korsunsky, 1996a; Salamon and Dundurs, 1971; Kolesnikova and Romanov, 2004). They are defined, with three parameters μ, v, λ and two (coordinate) variables ρ, ζ, as

$$J_{\mu,v;\lambda}(\rho,\zeta) = \int_0^\infty J_\mu(t) J_v(\rho t) \mathrm{e}^{-\zeta t} t^\lambda \, \mathrm{d}t \tag{9}$$

where $\rho = r/a$ and $\zeta = z/a$ and a is the radius of the dislocation. The functions $J_i(\cdot)$ are Bessel functions of the first kind. The integral exists for $\mu + v + \lambda > -1$ and $\zeta > 0$.

Eason et al. (1955) produced an invaluable and much cited, paper in which the Lipschitz–Hankel integrals are given in terms of combinations of complete Elliptic integrals. They only considered the Lipschitz–Hankel integrals in the restricted region in which $\zeta > 0$. This, in the present application, restricts the domain of applicability to the positive half space, and this is insufficient for our purposes. We therefore define a set of generalised Lipschitz–Hankel integrals, which are based on the definitions of Eason et al. but modified, where needed, to accomodate behaviour in the extended domain. They reduce to the standard form in the domain $\zeta > 0$.

A feature of these generalised integrals is that, for some combinations of the parameters, a discontinuity arises, as is required to achieve the physical discontinuity associated with the Burgers vector. These generalised Lipschitz–Hankel integrals we denote by $P_{\mu,v;\lambda}(\rho,\zeta,\alpha)$, where the additional variable, α, sets the angle that the path-cut line, which intersects the point $(\rho,\zeta) = (1,0)$, makes with the $z = 0$ plane.

Some of the significant properties are:

- When $\lambda \geqslant |\mu - v|$ the function is continuous, except for a point singularity at $(\rho,\zeta) = (1,0)$. The definitions of the Lipschitz–Hankel integrals needed no modification in this case.
- When $\lambda < |\mu - v|$ the function will have a line discontinuity, and the value of α becomes relevant, as we use it to set the orientation of the line of discontinuity. Modification of the definitions of the Lipschitz–Hankel integrals have been made in this case.
- When the sum of the parameters $\mu + v + \lambda$ is even the function is symmetric in ζ, and when odd the function is antisymmetric in ζ. This applies to both continuous and discontinuous cases, provided the discontinuity is on the $z = 0$ plane (thus $\alpha = 0$). The following relationship with the original Lipschitz–Hankel integrals applies

$$P_{\mu,v;\lambda}(\rho,\zeta,0) = \mathrm{sign}(\zeta)^{\mu+v+\lambda} J_{\mu,v;\lambda}(\rho,|\zeta|) \tag{10}$$

and indeed this limited modification was used by Korsunsky (1996a).

Appendix A gives explicit definitions of the generalised Lipschitz–Hankel integrals, for all those combinations of the parameters that we require. They are frequently referred to in the ensuing sections; in most cases the coordinate variables ρ, ζ have been omitted and only the α argument is retained, when relevant.

5. Dislocation solutions

In this section we list, initially without proof, the solutions as Papkovich–Neuber potentials together with displacement and stress fields. They are all given in terms of the generalised Lipschitz–Hankel integrals,

$P_{\mu,\nu;\lambda}(\rho,\zeta,\alpha)$, as defined in Appendix A. To differentiate the solutions the symbol for each component of the elastic field has been given a pre-subscript to denote the Burgers vector direction, and a superscript to denote the path cut orientation.

5.1. Radial dislocation; path cut exterior to disc (b_r^{o})

This result was given by Korsunsky, and is

Potentials

$$ {}_r\psi^{\mathrm{o}} = \mu a P_{0,0;-1}(0) b_r^{\mathrm{o}} \tag{11} $$

$$ {}_r\phi^{\mathrm{o}} = -\frac{2\mu}{(\kappa+1)} P_{0,0;0} b_r^{\mathrm{o}} \tag{12} $$

Displacements

$$ {}_r u_z^{\mathrm{o}} = -\frac{1}{\kappa+1}\left[\frac{\kappa-1}{2} P_{0,0;0} + \zeta P_{0,0;1}\right] b_r^{\mathrm{o}} \tag{13} $$

$$ {}_r u_r^{\mathrm{o}} = \frac{1}{\kappa+1}\left[\frac{\kappa+1}{2} P_{0,1;0}(0) - \zeta P_{0,1;1}\right] b_r^{\mathrm{o}} \tag{14} $$

Stress components

$$ {}_r\sigma_{zz}^{\mathrm{o}} = \frac{2\mu}{(\kappa+1)a}[\zeta P_{0,0;2}] b_r^{\mathrm{o}} \tag{15} $$

$$ {}_r\sigma_{rr}^{\mathrm{o}} = \frac{2\mu}{(\kappa+1)a}\left[2P_{0,0;1} - \zeta P_{0,0;2} + \frac{\zeta}{\rho} P_{0,1;1} - \frac{\kappa+1}{2\rho} P_{0,1;0}(0)\right] b_r^{\mathrm{o}} \tag{16} $$

$$ {}_r\sigma_{\theta\theta}^{\mathrm{o}} = \frac{2\mu}{(\kappa+1)a}\left(\frac{(3-\kappa)}{2} P_{0,0;1} - \frac{\zeta}{\rho} P_{0,1;1} + \frac{1}{\rho}\frac{(\kappa+1)}{2} P_{0,1;0}(0)\right) b_r^{\mathrm{o}} \tag{17} $$

$$ {}_r\sigma_{rz}^{\mathrm{o}} = \frac{2\mu}{(\kappa+1)a}[-P_{0,1;1} + \zeta P_{0,1;2}] b_r^{\mathrm{o}} \tag{18} $$

This solution was the main catalyst of the work presented here. In Korsunsky's paper he describes the displacement conditions as if the path cut is on the cylinder, but when his definitions of the Lipschitz–Hankel integrals are used the resulting solution is antisymmetric w.r.t. z with discontinuity for the radial displacement inversely proportional to radius along the $z = 0$ surface. Remote from the dislocation the displacements and stresses tend to zero.

5.2. Radial dislocation; path cut interior to disc (b_r^{i})

This result was published in part by Kolesnikova and Romanov (2004), who gave only the displacement and stress fields. It has similar form to Korsunsky's solution (see above), so allowing deduction of the potential functions.

Potentials

$$ {}_r\psi^{\mathrm{i}}(\rho,\zeta) = \mu a P_{2,0;-1}(0) b_r^{\mathrm{i}} \tag{19} $$

$$ {}_r\phi^{\mathrm{i}}(\rho,\zeta) = -\frac{2\mu}{(\kappa+1)} P_{2,0;0}(0) b_r^{\mathrm{i}} \tag{20} $$

Displacements

$$ {}_r u_z^{\mathrm{i}} = -\frac{1}{\kappa+1}\left[\frac{\kappa-1}{2} P_{2,0;0}(0) + \zeta P_{2,0;1}(0)\right] b_r^{\mathrm{i}} \tag{21} $$

$$ {}_r u_r^{\mathrm{i}} = \frac{1}{\kappa+1}\left[\frac{\kappa+1}{2} P_{2,1;0}(0) - \zeta P_{2,1;1}\right] b_r^{\mathrm{i}} \tag{22} $$

Stress components

$$ {}_r\sigma^{\mathrm{i}}_{zz} = \frac{2\mu}{(\kappa+1)a}[\zeta P_{2,0;2}]b^{\mathrm{i}}_r \tag{23} $$

$$ {}_r\sigma^{\mathrm{i}}_{rr} = \frac{2\mu}{(\kappa+1)a}\left[2P_{2,0;1}(0) - \zeta P_{2,0;2} + \frac{\zeta}{\rho}P_{2,1;1} - \frac{\kappa+1}{2\rho}P_{2,1;0}(0)\right]b^{\mathrm{i}}_r \tag{24} $$

$$ {}_r\sigma^{\mathrm{i}}_{\theta\theta} = \frac{2\mu}{(\kappa+1)a}\left(\frac{(3-\kappa)}{2}P_{2,0;1}(0) - \frac{\zeta}{\rho}P_{2,1;1} + \frac{1}{\rho}\frac{(\kappa+1)}{2}P_{2,1;0}(0)\right)b^{\mathrm{i}}_r \tag{25} $$

$$ {}_r\sigma^{\mathrm{i}}_{rz} = \frac{2\mu}{(\kappa+1)a}[-P_{2,1;1} + \zeta P_{2,1;2}]b^{\mathrm{i}}_r \tag{26} $$

As with the above solution, remote from the dislocation, the displacements and stresses decay to zero.

5.3. Radial dislocation; path cut on cylindrical surface (b^{c}_r)

This solution, in terms of Papkovich–Neuber potentials, is the main new finding. It is a linear combination of the above two solutions and an additional remote traction. The path cut is the cylinder surface with the discontinuities of the generalised Lipschitz–Hankel integrals set to coincide ($\alpha = \pi/2$). The physical nature of the combination can be considered as follows:

- The exterior cut solution (b^{o}_r), but now with the path cut set on the cylindrical surface, produces a solution which is equivalent to making a physical tubular cut, then applying traction to *only* the outer surface sufficient to create a radial displacement of b^{o}_r from the inner surface.
- The inner cut solution (b^{i}_r), but now with the path cut set on the cylindrical surface, produces a solution which is equivalent to making a physical tubular cut, then applying traction to *only* the inner surface sufficient to create a radial displacement of b^{i}_r from the outer surface.

In the latter case the inner material is "extruded" by the Poisson effect causing an axial stress and displacement of material. As we have not "glued" the material back together, this displacement would be unrestrained. To provide the necessary restraint an additional component is required. This is in the form of a traction in the negative z direction applied remotely to the central core to counter the extrusion.

The required proportions of the three solutions are dictated by the ratios of the displacements and stresses found in the field remote from the dislocation core ($z \to \infty$). These proportions are most easily found by considering, in plane strain, a ring of material added into the plane of the analysis. Material inside the ring displaces inwards, by an amount proportional to radius, and outside the ring it displaces outwards, by an amount inversely proportional to radius. The resulting (compressive) stress field decays as $1/r^2$ outside the ring but is constant inside the ring, including a non-zero axial component (σ_{zz}). The following table gives the components of stress and displacement of the plane strain solution when a ring of radius a and thickness δ is inserted.

	Inner $r < a$	Outer $r > a$
u_r	$-(\kappa-1)\frac{r\delta}{a(\kappa+1)}$	$2\frac{a\delta}{r(\kappa+1)}$
σ_{rr}	$-2\frac{2\mu\delta}{a(\kappa+1)}$	$-2\frac{2\mu a\delta}{r^2(\kappa+1)}$
σ_{zz}	$-(3-\kappa)\frac{2\mu\delta}{a(\kappa+1)}$	0
$\sigma_{\theta\theta}$	$-2\frac{2\mu\delta}{a(\kappa+1)}$	$2\frac{2\mu a\delta}{r^2(\kappa+1)}$

The axial stress is the remaining component to be adjusted, reflecting a far field traction not found in the above dislocation solutions. First we give the solution for this traction alone.

5.3.1. Distributed axial force

The Kelvin problem is a point force applied at an interior point of an infinite space. When the force is applied at the origin, in the direction of positive z, it has a Papkovich–Neuber potential solution given by

$$\phi = \frac{F}{2\pi(\kappa+1)R}, \tag{27}$$

where F is the concentrated force and R is the distance from its point of application to the point of observation; note that only the z direction vector Papkovich–Neuber potential is required. We require to integrate this solution in order to distribute it over a disc, with f representing the force density (σ_{zz}) on the internal circular surface, so that

$${}_K\phi = \frac{f}{2\pi(\kappa+1)} \int_{\text{disc}} \frac{q(r)\,\mathrm{d}A}{R} \tag{28}$$

and the result is found (see Appendix B for details of the integration) to be

$${}_K\phi = \frac{f\ a}{(\kappa+1)} P_{1,0;-1}(\rho,\zeta,0). \tag{29}$$

The pre-subscript K has been introduced to show that it is derived from the solution to Kelvin's problem.

This solution would normally be considered as having a path cut on the disc plane ($\alpha = 0$), where the traction is applied. When the path cut is along the cylindrical surface ($\alpha = \pi/2$) we find the elastic field caused by a remote traction on the central core, as if the cylindrical walls were tied radially but frictionless axially. The resulting elastic fields are:

Displacements

$${}_K u_z^{\mathrm{c}} = \frac{f\ a}{2\mu(\kappa+1)} [\kappa P_{1,0;-1}(\pi/2) + \zeta P_{1,0;0}(\pi/2)] \tag{30}$$

$${}_K u_r = \frac{f\ a}{2\mu(\kappa+1)} z P_{1,1;0} \tag{31}$$

Stress components

$${}_K\sigma_{zz}^{\mathrm{c}} = \frac{f\ a}{(\kappa+1)} \left[-\frac{\kappa+1}{2} P_{1,0;0}(\pi/2) - \zeta P_{1,0;1} \right] \tag{32}$$

$${}_K\sigma_{rr}^{\mathrm{c}} = \frac{fa}{(\kappa+1)} \left[-\frac{3-\kappa}{2} P_{1,0;0}(\pi/2) + \zeta P_{1,0;1} - \frac{\zeta}{\rho} P_{1,1;0} \right] \tag{33}$$

$${}_K\sigma_{\theta\theta}^{\mathrm{c}} = \frac{f\ a}{(\kappa+1)} \left[-\frac{3-\kappa}{2} P_{1,0;0}(\pi/2) + \frac{\zeta}{\rho} P_{1,1;0} \right] \tag{34}$$

$${}_K\sigma_{rz} = \frac{f\ a}{(\kappa+1)} \left[-\frac{\kappa-1}{2} P_{1,1;0} - \zeta P_{1,1;1} \right] \tag{35}$$

5.3.2. Composite solution

Finally, the composite solution, with the separate components left unexpanded is as follows:

Potentials

$${}_r\psi^{\mathrm{c}} = \left[\frac{\kappa-1}{\kappa+1} {}_r\psi^{\mathrm{i}} + \frac{2}{\kappa+1} {}_r\psi^{\mathrm{o}} \right] b_r^{\mathrm{c}} \tag{36}$$

$${}_r\phi^{\mathrm{c}} = \left[\frac{\kappa-1}{\kappa+1} {}_r\phi^{\mathrm{i}} + \frac{2}{\kappa+1} {}_r\phi^{\mathrm{o}} - \frac{2\mu(3-\kappa)}{a(\kappa+1)} {}_K\phi^{\mathrm{c}} \right] b_r^{\mathrm{c}} \tag{37}$$

There is no ${}_K\psi^c$ term because it is zero. Also note the factor of $2\mu/a$ which reflects that the distributed Kelvin solution originates from a specified traction rather than a displacement.

The solutions are linear, so, the resulting displacement and stress fields are found by adding the three components in identical proportion to the potentials.

Displacements

$$ {}_{r}u_k^{\mathrm{c}} = \frac{\kappa-1}{\kappa+1}\,{}_{r}u_k^{\mathrm{i}} + \frac{2}{\kappa+1}\,{}_{r}u_k^{\mathrm{o}} - \frac{2\mu(3-\kappa)}{a(\kappa+1)}\,{}_{K}u_k^{\mathrm{c}}, \quad k = r, z \tag{38} $$

Stress components

$$ {}_{r}\sigma_{ij}^{\mathrm{c}} = \frac{\kappa-1}{\kappa+1}\,{}_{r}\sigma_{ij}^{\mathrm{i}} + \frac{2}{\kappa+1}\,{}_{r}\sigma_{ij}^{\mathrm{o}} - \frac{2\mu(3-\kappa)}{a(\kappa+1)}\,{}_{K}\sigma_{ij}^{\mathrm{c}}, \quad ij = rr, zz, \theta\theta, rz \tag{39} $$

In practical application these formulae would be expanded and terms collected to reduce the number of special function valuations required.

5.4. Prismatic dislocation; path cut interior to disc (b_z^{i})

This result was also mentioned by Kolesnikova and Romanov (2004), but only Korsunsky (1996a) gives it in terms of potential functions. The path cut of the Lipschitz–Hankel integrals must be specified with $\alpha = 0$ because the physical cut is on the ($\zeta = 0$) disc surface.

Potentials

$$ {}_{z}\psi^{\mathrm{i}}(\rho,\zeta) = \frac{2\mu}{(\kappa+1)}\,\frac{(\kappa-1)}{2}\,aP_{1,0;-1}(\rho,\zeta,0)b_z^{\mathrm{i}} \tag{40} $$

$$ {}_{z}\phi^{\mathrm{i}}(\rho,\zeta) = -\frac{2\mu}{(\kappa+1)}P_{1,0;0}(\rho,\zeta,0)b_z^{\mathrm{i}} \tag{41} $$

Displacements

$$ {}_{z}u_z^{\mathrm{i}}(\rho,\zeta) = -\frac{1}{\kappa+1}\left[\frac{\kappa+1}{2}P_{1,0;0}(\rho,\zeta,0) + \zeta P_{1,0;1}\right]b_z^{\mathrm{i}} \tag{42} $$

$$ {}_{z}u_r^{\mathrm{i}}(\rho,\zeta) = \frac{1}{\kappa+1}\left[\frac{\kappa-1}{2}P_{1,1;0} - \zeta P_{1,1;1}\right]b_z^{\mathrm{i}} \tag{43} $$

Stress components

Note that, as this is a Volterra dislocation, these are not affected by the path cut:

$$ {}_{z}\sigma_{zz}^{\mathrm{i}}(\rho,\zeta) = \frac{2\mu}{(\kappa+1)a}[P_{1,0;1} + \zeta P_{1,0;2}]b_z^{\mathrm{i}} \tag{44} $$

$$ {}_{z}\sigma_{rr}^{\mathrm{i}}(\rho,\zeta) = \frac{2\mu}{(\kappa+1)a}\left[P_{1,0;1} - \zeta P_{1,0;2} + \frac{\zeta}{\rho}P_{1,1;1} - \frac{\kappa-1}{2\rho}P_{1,1;0}\right]b_z^{\mathrm{i}} \tag{45} $$

$$ {}_{z}\sigma_{\theta\theta}^{\mathrm{i}}(\rho,\zeta) = \frac{2\mu}{(\kappa+1)a}\left[\frac{3-\kappa}{2}P_{1,0;1} - \frac{\zeta}{\rho}P_{1,1;1} + \frac{1}{\rho}\,\frac{\kappa-1}{2}P_{1,1;0}\right]b_z^{\mathrm{i}} \tag{46} $$

$$ {}_{z}\sigma_{rz}^{\mathrm{i}}(\rho,\zeta) = \frac{2\mu}{(\kappa+1)a}[\zeta P_{1,1;2}]b_z^{\mathrm{i}} \tag{47} $$

5.5. Prismatic dislocation; path cut on cylindrical surface (b_z^{c})

Here the path cut of the Lipschitz–Hankel integrals must be specified as $\alpha = \pi/2$, as the physical cut is on the ($\rho = 1$) cylinder.

Potentials

$$ \psi_z^{\mathrm{c}}(\rho,\zeta) = \frac{2\mu}{(\kappa+1)}\,\frac{(\kappa-1)}{2}\,aP_{1,0;-1}\left(\rho,\zeta,\frac{\pi}{2}\right)b_z^{\mathrm{c}} \tag{48} $$

$$ \phi_z^{\mathrm{c}}(\rho,\zeta) = -\frac{2\mu}{(\kappa+1)}P_{1,0;0}\left(\rho,\zeta,\frac{\pi}{2}\right)b_z^{\mathrm{c}} \tag{49} $$

All displacement and stress components are identical to those for the climb dislocation (above), except the z-direction displacement, which is now given by

$$ {}_z u_z^{\mathrm{c}}(\rho,\zeta) = -\frac{1}{\kappa+1}\left[\frac{\kappa+1}{2}P_{1,0;0}\left(\rho,\zeta,\frac{\pi}{2}\right)+\zeta P_{1,0;1}(\rho,\zeta)\right]b_z^{\mathrm{c}} \tag{50} $$

As this dislocation is Volterra in nature we are not restricted and the path cut may be set at any angle, which is not true for the radial dislocations.

6. Validity of the solutions

As the solutions are based on Papkovich–Neuber potential functions we know that the elastic field equations (equilibrium, compatibility) are valid provided the potential functions are harmonic. Application of the Laplace operator to the Lipschitz–Hankel integrals gives:

$$ \nabla^2 J_{\mu,\nu;\lambda} = \frac{\nu^2}{r^2}J_{\mu,\nu;\lambda} \tag{51} $$

so, when $\nu = 0$ the Lipschitz–Hankel integrals are harmonic and may be used as potential functions, which is the case for all the functions encountered in this paper.

The solutions are relevant to an infinite medium, and hence there are no "boundary conditions" to be satisfied remotely, but it is important that the solutions display the correct continuity and discontinuity along the path cut. That this is so is demonstrated for two example solutions, and it can be verified that the remainder of the solutions display the correct properties in a similar manner.

6.1. Prismatic dislocation; path cut interior to disc (b_z^{i})

6.1.1. Displacements

The axial displacement field for this dislocation is given in Eq. (42), above, and is required to display the discontinuity specified in Eq. (4). So, substituting in and simplifying we get

$$ \lim_{\epsilon\to 0}(u_z(\rho<1,+\epsilon)-u_z(\rho<1,-\epsilon)) = b_z^{\mathrm{i}}\lim_{\zeta\to 0}\left(P_{1,0;0}(\rho<1,\zeta,0)+\frac{2\zeta}{\kappa+1}P_{1,0;1}\right) \tag{52} $$

From the properties of the generalised Lipschitz–Hankel integrals, given above: $P_{1,0;1}$ is continuous, and thus the product $\zeta P_{1,0;1}$ will tend to zero, whilst $P_{1,0;0}$ is anti-symmetric and discontinuous at $z = 0$. We need only find the value of $P_{1,0;0}$ as $\zeta \to 0$. Salamon and Walter (1979) considered the limiting value of the Lipschitz–Hankel integrals and give the following result

$$ \lim_{\zeta\to 0}(J_{1,0;0}) = \begin{cases} 1 & \rho < 1 \\ \frac{1}{2} & \rho = 1 \\ 0 & \rho > 1 \end{cases} \tag{53} $$

which, on noting the equivalence of P and J in this case Eq. (10), gives the result we seek – a discontinuity in u_z of b_z^{i} within the disc ($\rho < 1$), and zero outside the disc ($\rho > 1$).

The radial displacement must show no discontinuity. Note that all the Lipschitz–Hankel integrals in the expression for radial displacement, given above in Eq. (43), are all continuous, as in each case $\lambda \geqslant |\mu - \nu|$, so the condition is met.

6.1.2. Stress components

We need only consider the components of the traction on the path cut surface: $z = 0$ viz. σ_{zz} and σ_{rz}, and they are given above in Eqs. (44) and (47). As with the radial displacement we only need check the parameters of the constituent Lipschitz–Hankel integrals; again the requirement for continuity is met, as in each case $\lambda \geqslant |\mu - \nu|$.

6.2. Radial dislocation; path cut on the cylinder (b_r^c)

6.2.1. Displacements

The required radial displacement discontinuity is specified in Eq. (3). The radial displacement is given in Eq. (38) and when the component solutions are substituted and after some manipulation, this results in:

$$ {}_r u_r^c = \frac{b_r^c}{\kappa+1} \left\{ \begin{array}{c} -\frac{\kappa+1}{2} P_{0,1;0} + (\kappa-1) P_{1,1;-1} \\ +\zeta P_{1,1;0} + \zeta(\kappa+1) P_{0,1;1} \end{array} \right\} \tag{54} $$

The Lipschitz–Hankel integrals $P_{1,1;0}$, and $P_{0,1;1}$ are continuous, and when $\alpha = \pi/2$, $P_{1,1;-1}$ is also continuous at $\rho = 1$ (its discontinuity is a only change of gradient). When the remaining significant parts are substituted into the displacement condition, Eq. (3) we are left with

$$ \lim_{\epsilon \to 0} (u_r(1+\epsilon, \zeta > 0) - u_r(1-\epsilon, \zeta > 0)) = b_r^c \left[-\frac{1}{2} P_{0,1;0}\left(1+\epsilon, \zeta, \frac{\pi}{2}\right) + \frac{1}{2} P_{0,1;0}\left(1-\epsilon, \zeta, \frac{\pi}{2}\right) \right] \tag{55} $$

Now consult Appendix A where it is found there is a discontinuity, in $P_{0,1;0}$, at $\rho = 1$ of -2, so providing the required dislocation.

There must be no discontinuity in the axial displacement. Substituting in the component solutions to Eq. (38) and manipulating, results in

$$ {}_r u_z^c = \frac{b_r^c}{\kappa+1} \left\{ -\frac{3-\kappa}{2} P_{0,0;0} + \zeta P_{0,0;1} + \rho P_{1,1;0} \right\} \tag{56} $$

All of these Lipschitz–Hankel integrals are continuous ($\lambda \geqslant |\mu - \nu|$), so the displacement will be also, as required.

6.2.2. Stress field

Expanding out the relevant stresses from Eq. (39) we obtain, for the shear stress

$$ {}_r \sigma_{rz}^c = \frac{2\mu}{a(\kappa+1)} \left[P_{0,1;1} - \zeta P_{0,1;2} - \frac{\kappa-1}{2} P_{1,1;0} + \zeta P_{1,1;1} \right] \tag{57} $$

As all the Lipschitz–Hankel integrals are continuous so continuity of the stress field is satisfied. For the radial stress we obtain

$$ {}_r \sigma_{rr}^c = \frac{2\mu}{a(\kappa+1)} \left[\begin{array}{c} -2P_{0,0;1} + \zeta P_{0,0;2} - \frac{\zeta}{\rho} P_{0,1;1} - \zeta P_{1,0;1} + \frac{(\kappa+1)\zeta}{2\rho} P_{1,1;0} \\ +\frac{1}{\rho} P_{0,1;0} + P_{1,0;0} \end{array} \right] \tag{58} $$

The terms in the upper row are all continuous, and the remaining discontinuous terms, viz. $P_{1,0;0}$ and $P_{0,1;0}$, have equal and opposite discontinuities at $\rho = 1$, so cancelling each other out, giving a continuous radial stress field, as required. There is a distinct change of gradient, i.e. $\partial_r \sigma_{rr}^c / \partial r$ is discontinuous at $\rho = 1$.

7. Results and discussion

7.1. Elastic fields

The Somigliana ring dislocation solutions are presented in the form of plots. Due to the axially symmetric character of the problem it is sufficient to consider the fields within the (r, z) plane. Figs. 3–17 illustrate the elastic displacement and stress fields in the neighbourhood of the dislocation that intersects the (r, z) plane at point $(a, 0)$. As in the rest of the paper, all coordinates are normalised with respect to the ring radius a, i.e. coordinates $\rho = r/a$ and $\zeta = z/a$ are used.

The main feature of the displacement fields is the discontinuous nature of their variation across the path cut surfaces, with this discontinuous jump only affecting the displacement component that coincides in direction with the Burgers vector. Since it is difficult to deduce the nature of such discontinuity from a contour plot, the relevant displacement components were plotted in the form of a surface. The ''escarpments'' that appear on

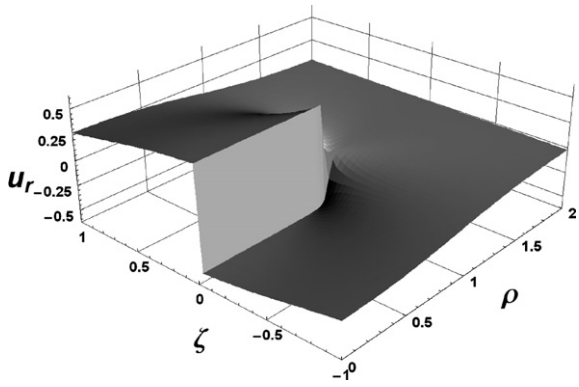

Fig. 3. Axial prismatic dislocation, axial displacement ${}_zu_z^i$.

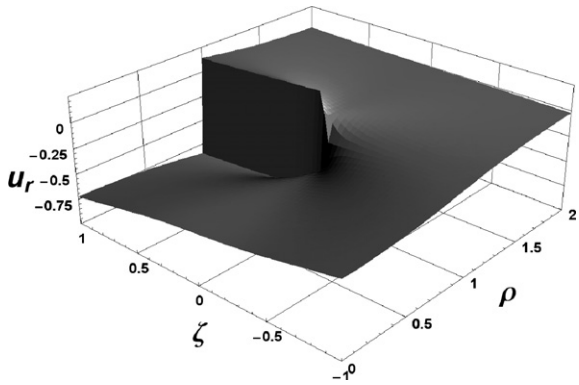

Fig. 4. Axial shear dislocation, axial displacement ${}_zu_z^c$.

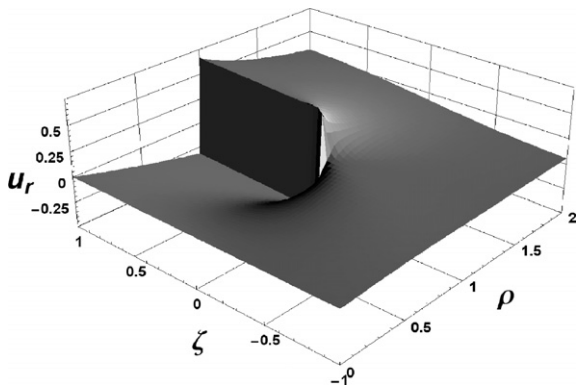

Fig. 5. Radial cylinder dislocation, radial displacement ${}_ru_r^c$.

the plots in Figs. 3–5 reveal clearly the nature of the discontinuity. The plot height has been normalized with respect to the magnitude of the Burgers vector.

For the axial dislocation both path cuts (Fig. 3 and 4) clearly show a displacement discontinuity that is constant along the path cut. This observation is also true for the radial discontinuity with a path cut on the surface of the cylinder $\rho = 1$ (Fig. 5). Although there exists an apparent similarity between the plots in Figs. 4 and 5, it is worth noting that radial displacement for the radial dislocation drops to zero at the axis $\rho = 0$.

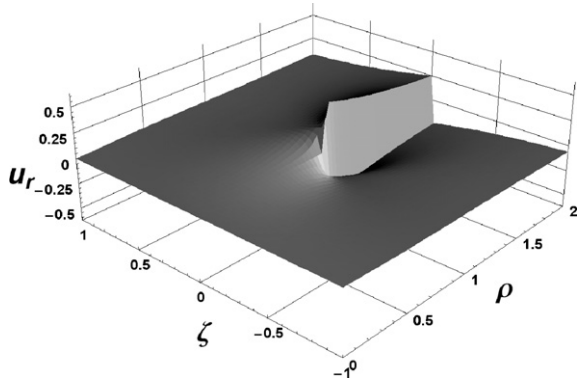

Fig. 6. Radial outer dislocation, radial displacement ${}_{r}u_r^{o}$.

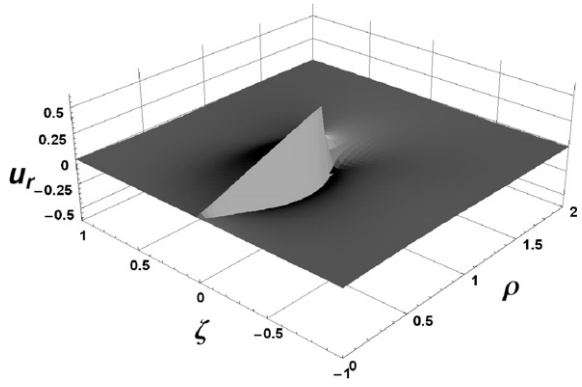

Fig. 7. Radial inner dislocation, radial displacement ${}_{r}u_r^{i}$.

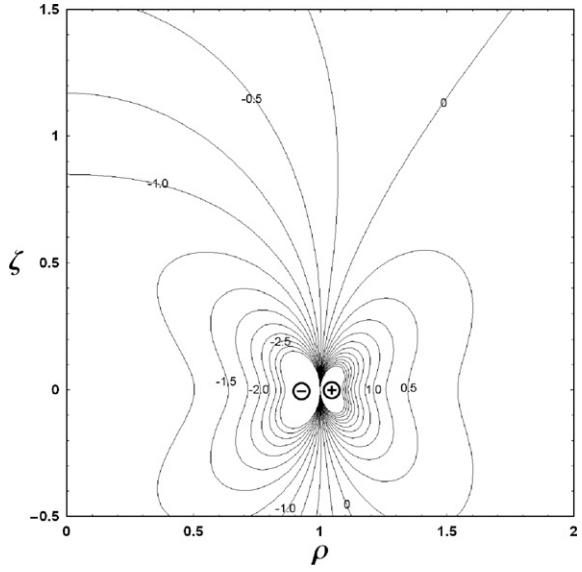

Fig. 8. Axial dislocation, axial direct stress ${}_{z}\sigma_{zz}$.

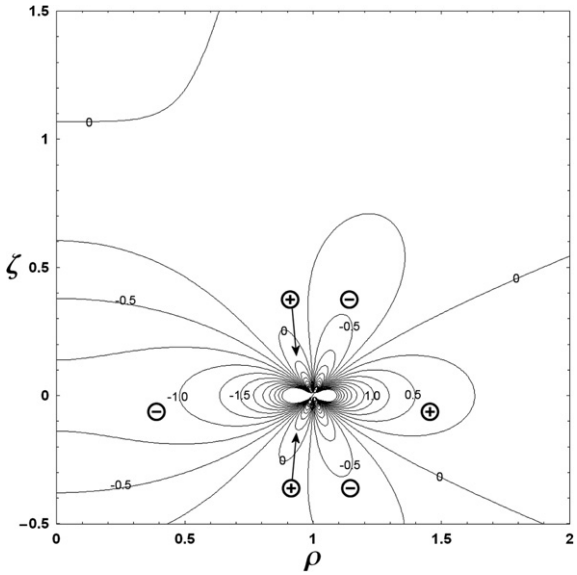

Fig. 9. Axial dislocation, radial direct stress ${}_z\sigma_{rr}$.

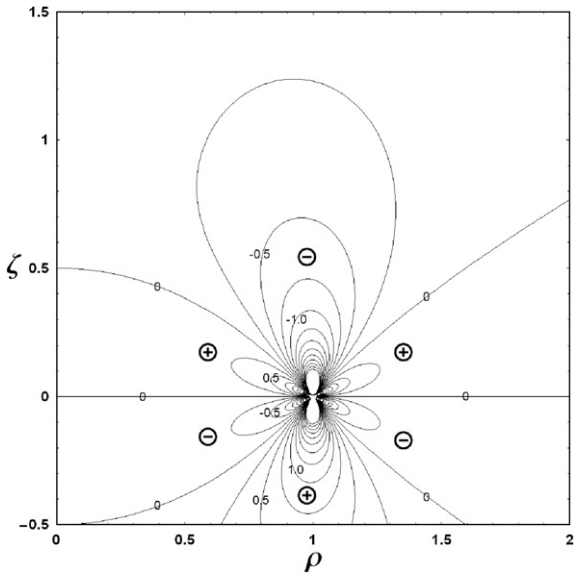

Fig. 10. Axial dislocation, shear stress ${}_z\sigma_{rz}$.

For the radial dislocation with the path cut on the cylindrical surface $r = 1$ (Fig. 5), the radial displacement varies linearly in the domain lying within the cylinder, $r < 1$, while outside this region it shows a gradual decay towards zero at large radial distance from the dislocation.

In Figs. 6 and 7 the two types of radial dislocation are considered with path cuts located on the plane $\zeta = 0$. The correct magnitudes of the radial displacement jump that must be prescribed in this case for the Inner and Outer radial shear dislocation solutions are, respectively, directly and inversely proportional to radius. These choices ensure that the radial component of displacement decays in all directions to zero at large distances from the dislocation line.

To summarise, surface plots of are shown in Figs. 3 and 4 for the axial dislocation and axial displacement component b_z, and in Figs. 5–7 for the radial dislocation and radial displacement component b_r. These plots

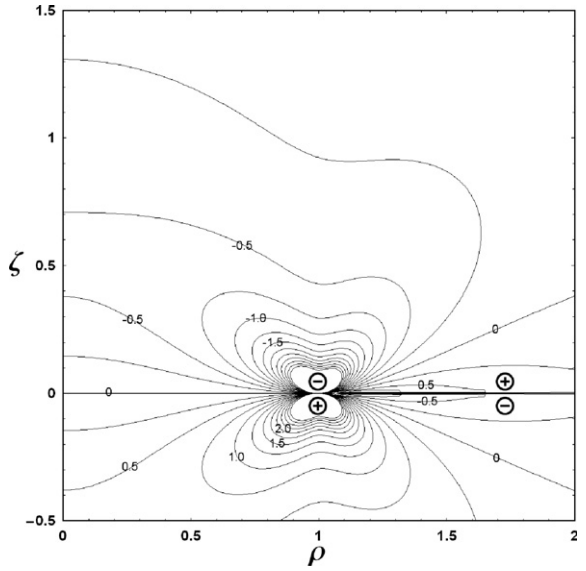

Fig. 11. Radial outer dislocation, radial direct stress ${}_r\sigma^{o}_{rr}$.

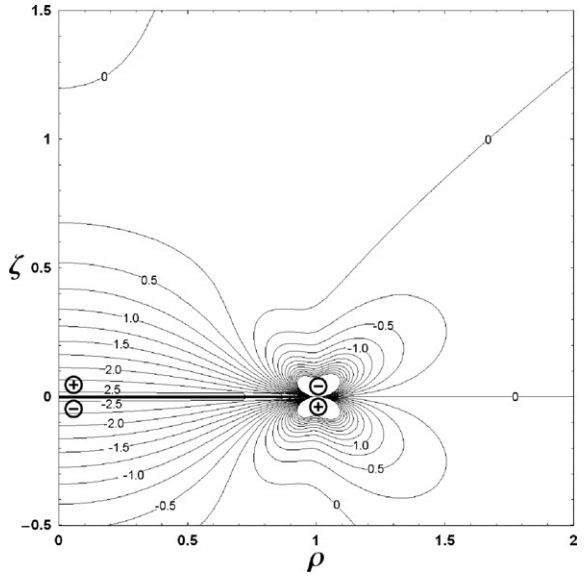

Fig. 12. Radial inner dislocation, radial direct stress ${}_r\sigma^{i}_{rr}$.

provide clear demonstration that the solutions are 'well-behaved', i.e. possess correct asymptotic behaviour at large values of ζ and ρ. The solution shown in Fig. 5 is perhaps particularly interesting, since it shows that the linear variation of displacement with radius persists within the region $\rho < 1$ to large positive values of ζ – a property never encountered for plane Volterra dislocations, and thus representing a crucial feature of the Somigliana solution for a dislocation with a spatially varying Burgers vector.

Stress fields around dislocations are illustrated with contour plots. The stress values shown on the contour labels have been normalized by the common factor of $2\mu b/(\kappa + 1)$. In addition "+" and "−" symbols have been placed on the contour maps to provide a clear indication of the stress sign within the regions between any two contour lines representing zero stress value.

Those familiar with the appearance of stress fields around plane Volterra dislocations would immediately be able to recognize certain features in these plots, particularly for the stress fields around the axial dislocation

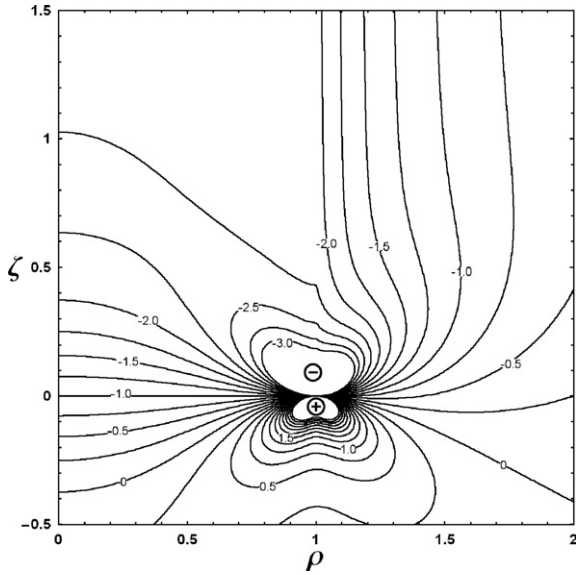

Fig. 13. Radial cylinder dislocation, radial direct stress ${}_r\sigma^{c}_{rr}$.

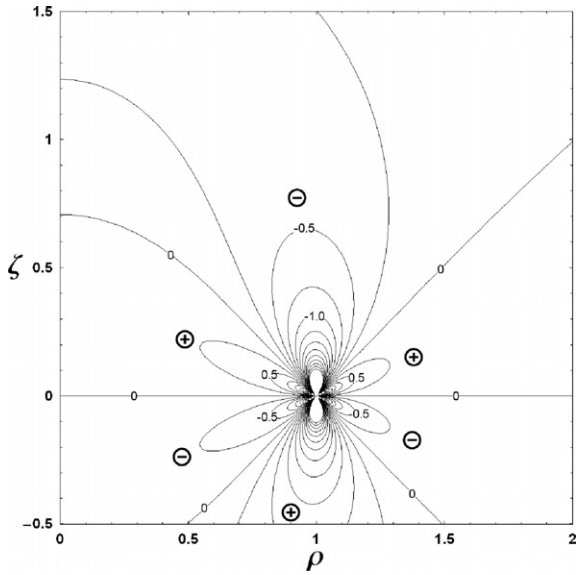

Fig. 14. Radial outer dislocation, axial direct stress ${}_r\sigma^{o}_{zz}$.

shown in Figs. 8–10. This is a consequence of the fact that the axial dislocation considered in these Figures is, in fact, a true Volterra dislocation, that is, however, bounded by a circular line of finite curvature. In this context the conventional plane Volterra dislocation can, of course, be thought of as the limiting case of the axial dislocation presented in Figs. 8–10 when the dislocation radius is made very large. On the normalized plots used here this corresponds to 'zooming in' into the region close to the dislocation line $\rho = 1$, $\zeta = 0$.

All stress fields shown in Figs. 8–10 are continuous, except for the expected point singularity at the dislocation core. They display the correct properties of symmetry (and anti-symmetry) about $\zeta = 0$, and also the correct behaviour as the axis of symmetry $\rho = 0$ approached.

Contour plots of stresses around radial dislocations with path cuts lying on the plane $\zeta = 0$ (Figs. 11–17) also display clear symmetry and anti-symmetry properties with respect to this plane. However, distinct differ-

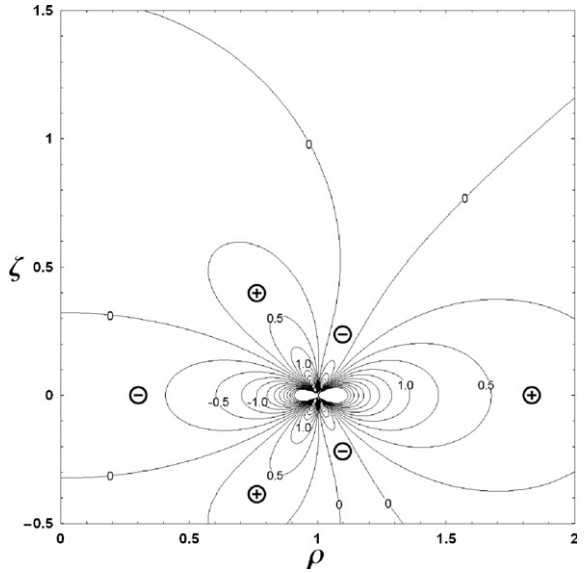

Fig. 15. Radial outer dislocation, shear stress ${}_r\sigma^{\mathrm{o}}_{rz}$.

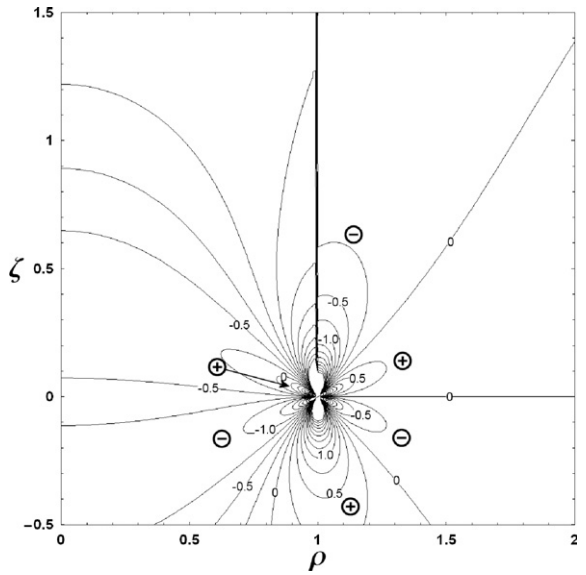

Fig. 16. Radial cylinder dislocation, axial direct stress ${}_r\sigma^{\mathrm{c}}_{zz}$.

ences from plane Volterra dislocation solutions can be observed in this case. Note that the radial direct stress (Figs. 11 and 12) exhibits a secondary zone of stress concentration that is most pronounced in the case of the inner path cut. Here just above the disc $\rho < 1$, $\zeta = 0$, the stress is positive with the magnitude $(7 - \kappa)/(\kappa + 1)$, and just below the disc it is negative with the same amount.

The radial dislocation obtained by the cylindrical cut shown in Fig. 13 is well behaved, since the combination of solutions used cancels out the secondary stress concentrations. The solution displays lack of symmetry for large positive and negative values of ζ. As $\zeta \to \infty$ the solution does not decay, but instead tends to a non-trivial solution of plane strain problem about inserting an extra circular layer of material of thickness b_r at $r = a$. Note that the radial stress component is continuous across the path cut, although it suffers a discontinuous change in gradient.

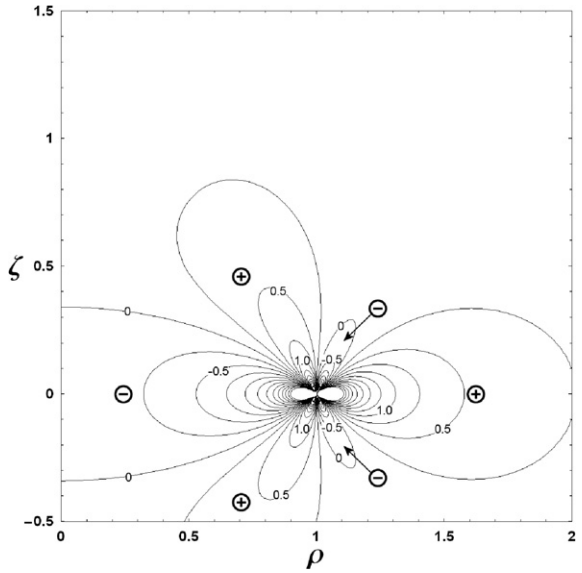

Fig. 17. Radial cylinder dislocation, shear stress ${}_r\sigma^c_{rz}$.

Contour plots of the axial and shear stress components shown in Figs. 14 and 15 are perhaps less remarkable, since they display greater similarity to their plane Volterra dislocation counterparts. Some asymmetric distortion can however be detected due to the presence of the axis of symmetry at $\rho = 0$. The contour plot of the axial stress component for the radial dislocation obtained with the help of a cylindrical cut illustrated in Fig. 16 shows some discontinuity across the cut line $\rho = 1$, $\zeta > 0$. Perhaps somewhat surprisingly, the shear stress arising around the radial dislocation obtained by the cylindrical path cut does not show any asymmetry (Fig. 17).

The discussion of surface and contour plots of displacements and stresses around Somigliana ring dislocations presented in this section demonstrates that these solutions possess greater variety and complexity than their plane Volterra counterparts. One of the most prominent conclusions that must be drawn on the basis of this analysis is that the nature of the displacement and stress–strain fields shows strong dependence on the path cut, and on the variation of displacement discontinuity along the path cut. Similar stress fields can be generated around a radial dislocation by employing solutions involving a cylindrical path cut, or path cuts lying in the bounded ($\rho < 1$) or unbounded ($\rho > 1$) parts of the plane. The choice of the dislocation type to be used in the analysis of a particular problem, e.g. involving a crack, must then depend on matching the nature of the problem to the nature of the fundamental solution used to 'assemble' the crack. The situation can be expected to go to a yet higher level of complexity if the cut surface is allowed to be no longer confined to a plane or cylindrical surface, so that e.g. path cuts lying on a truncated cone surface are considered.

7.2. Remarks on the conservation of Burgers vector and relevance of Frank's rule

It is perhaps appropriate to present here a discussion of the relationship between the kinds of dislocations considered in this paper, and the more conventional dislocation structures that have been observed in crystals and studied both experimentally and theoretically over many decades.

In classical texts on dislocation theory the greatest attention is devoted to the consideration of dislocations that, can occur in finite crystal structures, and are characterized by constant values of the Burgers vector, also known as dislocations of Volterra type.

In mathematical terms these can be readily visualised as arising due to rigid body displacement of one part of a solid body with respect to the other; or by assuming that displacements are given by a multi-valued function, and selecting a particular leaf of such a function. In his Treatise, Love (1927) presents a compelling historical and analytical note on the subject of Volterra dislocations in which he discusses how the possibility of

this physical phenomenon manifests itself in the displacement, strain and stress solutions within the theory of elasticity. The fundamental starting point for Love's discussion is the consideration of a multiply connected cylindrical region, because such a region admits the existence of multi-valued displacements. It is worth noting in passing that this approach bears a strong resemblance to the way in which the dislocation core needs to be excluded from consideration if elastic theory is to be used to analyse the state of self-stress induced by the presence of a dislocation. Love considers the possibility of making a cut along a radial plane and imposing a constant relative displacement between opposite faces of the cut in the axial, radial or hoop direction, removing or adding material if required. Love then notes that a multiply-connected region can be rendered simply connected by introducing a system of barriers, and proposes using the radial half plane bounded by the axis as such a barrier for the cylinder problem under consideration. He proceeds to prove a theorem, due to Cesàro, that expresses the conditions for strains and stresses to be single-valued, even though the displacements are no longer required to be. Love arrives at Weingarten's result that this requires that the displacement of one side of the cut with respect to the other must be a displacement that is possible in a rigid body.

Because of the fact that Volterra dislocations stand in a clear relationship with the physical entities encountered in crystals, certain properties can be deduced for them. One such property is conservation of Burgers vector, also known as Frank's rule (Weertman, 1996; Hurtado and Weertman, 1995). In Love's terminology, if the region of a solid has been rendered simply connected by a system of impenetrable barriers, then such barriers cannot terminate other than on the surface of the body, or at a dislocation line. This line, in turn, cannot terminate within the body, and must also emerge at the body surface. The only remaining alternative is for the line to branch. Such a phenomenon is indeed observed in crystals, and is known as a dislocation junction. Frank's rule follows from Love's result that only constant rigid body displacements are allowed between constituent parts of the solid body: if that requirement is enforced, the difference in displacement between parts must be preserved, and so too must be the Burgers vector.

Most of the dislocation entities considered in the present paper are, however, of Somigliana, and not of Volterra type. In these dislocations relative displacements of the cut faces are allowed to vary with position. Nevertheless, the principles of constructing the resulting self-equilibrated stress fields are entirely similar to those outlined by Love, and involve relative displacement, renewed bonding of cut surfaces and possible material removal when required. Consider, for example, the problem involving cutting out an infinitely long cylinder out of an unbounded elastic space, adding a layer of material to its surface, inserting it back in place, and re-establishing the bond. By construction, this is a dislocation-like entity, and it does, indeed, give rise to a single-valued self-equilibrating stress field. However, there is not a dislocation line in sight, and making a Burgers circuit presents a problem. For the Somigliana dislocations considered dislocation lines exist in the form of circular loops. However, in some cases self-equilibrated stress fields persist to infinitely large distances from these circuits, similar to the infinite cylinder problem sketched above, and indicating that the usual treatment procedures based on Burgers vector analysis may not be able to capture the resulting elastic fields.

In the present study our primary concern was to compute, in a way as transparent and concise as possible, the displacement and stress fields associated with circular Somigliana dislocations. For this purpose we selected Papkovich–Neuber potentials as a suitable vehicle, since they allowed the results to be expressed in analytical form with the help of the so-called Lipschitz–Hankel integrals.

Weertman (1996) and Hurtado and Weertman (1995) present a powerful framework for the analysis of complex dislocation structures that is based on the concept of infinitesimal surface dislocation density fields associated with curved dislocation lines, for which Burgers vector direction varies along the line. This approach may provide an interesting means of representing the Somigliana dislocations considered in terms of spatially varying fields of edge and slip dislocations distributed on appropriately selected surfaces. The application of this approach is likely to produce additional insight into the properties of ring Somigliana dislocations, but would require the development of a substantial set of tools. Therefore, it is the authors' belief that it deserves a separate study.

8. Conclusion

The study presented in this paper was motivated by the desire to address axisymmetric crack problems using the distributed dislocation technique. While it seems possible to employ the methodologies developed

and applied successfully to a wide variety of plane crack problems, it becomes apparent in the case of ring dislocations that the relevant family of solutions possesses a much higher level of complexity. In particular, the solutions display a clear dependence on the choice of path cut that is not allowed for Volterra dislocations.

It must be concluded, then, that in order to tackle axisymmetric crack problems, the choice of correct dislocation solution must be made at the outset. For torsionless problems considered here only two classes of circular edge dislocation are relevant. The first class consists of the axial prismatic dislocations of the Volterra type that induce a state of stress independent of the path-cut. The second class consists of the radial dislocation of the Somigliana type, i.e. a generalised dislocation solution for which the state of stress induced in the body depends on the path cut chosen.

Solutions have been presented here in the form of formulae and some surface and contour plots. This, however, does not make it easy for other researchers to use them, since copying of the formulae often leads to the introduction of errors, indeed some of the papers referred to had typographical errors that caused subsequent problems. Hopefully this will reduced by the fact that modern electronic publication removes most of the chances of errors in the typsetting of formulae.

Acknowledgements

The authors would like to thank the following colleagues: Prof. A. Sackfield (Nottingham Trent University) for assistance with some of the Lipschitz–Hankel integral definitions and Prof. J.R. Barber (University of Michigan) for discussion on the mechanics of candidate solutions.

Appendix A. Generalised Lipschitz–Hankel integrals

At the core of the dislocation kernels are the Lipschitz–Hankel integrals. The standard definition is as an integral of the product of Bessel functions, an exponential and a power; we will be using the definition with normalised coordinate variables

$$J_{\mu,\nu;\lambda}(\rho,\zeta)=\int_0^\infty J_\mu(t)J_\nu(\rho t)\mathrm{e}^{-\zeta t}t^\lambda\,\mathrm{d}t$$

where $\rho=r/a$, $\zeta=z/a$. This integral exists for: $\mu+\nu+\lambda>-1$, $\rho\geqslant 0$ (the radial coordinate) and $\zeta>0$ (the axial coordinate). Eason et al. (1955) gives a comprehensive review of their properties and show how they can be expressed in terms of complete Elliptic Integrals. Eason et al. maintain the restriction of $\zeta>0$, but we have extended their region of validity by adopting their definitions, using them for all ζ and when required, making modification to control the discontinuities that occur in some combinations of the parameters.

Complete Elliptic Integrals exist for all of the $\rho-\zeta$ region but do have singularities and discontinuities. We use the following common forms for the definitions for the complete Elliptic integrals 1st, 2nd, 3rd kinds

$$\mathbf{K}=\int_0^{\pi/2}\frac{\mathrm{d}\theta}{\sqrt{1-k^2\sin^2\theta}} \tag{A.1}$$

$$\mathbf{E}=\int_0^{\pi/2}\sqrt{1-k^2\sin^2\theta}\,\mathrm{d}\theta \tag{A.2}$$

$$\mathbf{\Pi}=\int_0^{\pi/2}\frac{\mathrm{d}\theta}{(1-h\sin^2\theta)\sqrt{1-k^2\sin^2\theta}} \tag{A.3}$$

the variables of these integrals are called the: *modulus* (k), *complementary modulus* (k') and the *parameter* (h):

$$k=\sqrt{\frac{4\rho}{(\rho+1)^2+\zeta^2}},\quad k'=\sqrt{1-k^2},\quad h=\frac{4\rho}{(\rho+1)^2} \tag{A.4}$$

(note that the sign of all these is independent of ζ). These expressions are used in the definitions of the Lipschitz–Hankel integrals.

A.1. The definitions

First, this is a list of the Lipschitz–Hankel integrals occurring in the solutions of the paper (an asterisk is placed next to those that show a discontinuity):

$$\begin{array}{lllll} P_{0,0;-1^*} & P_{0,0;0} & P_{0,0;1} & P_{0,0;2} & \\ P_{1,0;-1^*} & P_{1,0;0^*} & P_{1,0;1} & P_{1,0;2} & P_{1,1;-1^*} \\ P_{2,0;-1^*} & P_{2,0;0^*} & P_{2,0;1^*} & P_{2,0;2} & \end{array} \qquad \begin{array}{lll} P_{0,1;0^*} & P_{0,1;1} & P_{0,1;2} \\ P_{1,1;0} & P_{1,1;1} & P_{1,1;2} \\ P_{2,1;0^*} & P_{2,1;1} & P_{2,1;2} \end{array}$$

For each of the definitions we indicate in which dislocation component(s) it occurs in, using the system of super- and sub-scripts used in the main text.

Note that, in several of the dislocation formulae the Lipschitz–Hankel integrals occur divided by radius. This only occurs when $\nu = 1$. To avoid evaluation difficulties on the axis ($\rho = 0$) a separate expression has been found and is given in the formulae below.

$P_{0,0;-1}$ occurs in: ${}_r\phi^{\circ}$

This formally cannot be evaluated, because: $\mu + \nu + \lambda \not> -1$. When used in the displacement or stress fields it is always differentiated (then this sum increases) so this is not a problem.

$P_{0,0;0}$ occurs in: ${}_r u_z^{\circ}$

$$P_{0,0;0}(\rho,\zeta) = \frac{k}{\pi\sqrt{\rho}}\mathbf{K} \tag{A.5}$$

$P_{0,0;1}$ occurs in: ${}_r u_z^{\circ}, {}_r\sigma_{rr}^{\circ}, {}_r\sigma_{\theta\theta}^{\circ}$

$$P_{0,0;1}(\rho,\zeta) = \frac{k^3\zeta}{4\pi\rho^{3/2}k'^2}\mathbf{E} \tag{A.6}$$

$P_{0,0;2}$ occurs in: ${}_r\sigma_{rr}^{\circ}, {}_r\sigma_{zz}^{\circ}$

$$P_{0,0;2}(\rho,\zeta) = \frac{k^5}{16\pi\rho^{5/2}k'^2}\left(\left(\frac{2\left(1+k'^2\right)}{k'^2} - \frac{4\rho}{k^2}\right)\mathbf{E} - \zeta^2\mathbf{K}\right) \tag{A.7}$$

$P_{0,1;0}$ occurs in: ${}_r u_r^{\circ}, {}_r\sigma_{rr}^{\circ}, {}_r\sigma_{\theta\theta}^{\circ}$

$$P_{0,1;0}(\rho,\zeta,\alpha) = -\frac{k\zeta}{2\pi\rho^{3/2}}\left(\mathbf{K} + \frac{\rho-1}{\rho+1}\mathbf{\Pi}\right) + \operatorname{sign}\left(\arctan\frac{\zeta}{|\rho-1|} - \alpha\right)\begin{cases} 0 & \rho < 1 \\ 1/2 & \rho = 1 \\ 1/\rho & \rho > 1 \end{cases}$$

$$\left.\frac{P_{0,1;0}(\rho,\zeta)}{\rho}\right|_{\rho=0} = \frac{1}{2}\zeta\left(\frac{1}{1+\zeta^2}\right)^{\frac{3}{2}} \tag{A.8}$$

$P_{0,1;1}$ occurs in: ${}_r u_r^{\circ}, {}_r\sigma_{rr}^{\circ}, {}_r\sigma_{rz}^{\circ}, {}_r\sigma_{\theta\theta}^{\circ}$

$$P_{0,1;1}(\rho,\zeta) = \frac{k}{2\pi\rho^{3/2}}\left(\mathbf{K} - \frac{\zeta^2+1-\rho^2}{\zeta^2+(1-\rho)^2}\mathbf{E}\right) \tag{A.9}$$

$$\left.\frac{P_{0,1;1}(\rho,\zeta)}{\rho}\right|_{\rho=0} = \frac{1}{2}(2\zeta^2-1)\left(\frac{1}{1+\zeta^2}\right)^{\frac{5}{2}} \tag{A.10}$$

$P_{0,1;2}$ occurs in: ${}_r\sigma_{rz}^{\circ}$

$$P_{0,1;2}(\rho,\zeta) = \frac{k^3\zeta}{8\pi k'^2\rho^{5/2}}\left(\left(\frac{k^4\left(\rho^4 - \left(\zeta^2+1\right)^2\right)}{4k'^2\rho^2} + 3\right)\mathbf{E} - \frac{k^2\left(\rho^2-\zeta^2-1\right)}{4\rho}\mathbf{K}\right) \tag{A.11}$$

$$\left.\frac{P_{0,1;2}(\rho,\zeta)}{\rho}\right|_{\rho=0} = \frac{3}{2}\left(2\zeta^2-3\right)\left(\frac{1}{1+\zeta^2}\right)^{\frac{7}{2}} \tag{A.12}$$

$P_{1,0;-1}$ occurs in: ${}_K\mathrm{u}_z$, ${}_z\psi^i$, ${}_K\phi$

$$P_{1,0;-1}(\rho,\zeta,\alpha) = \frac{1}{2\pi\sqrt{\rho}}\left[\frac{4\rho}{k}\mathbf{E} + (1-\rho^2)k\mathbf{K} + k\zeta^2\frac{1-\rho}{1+\rho}\mathbf{\Pi}\right] \tag{A.13}$$

$$-\zeta\,\mathrm{sign}\left(\arctan\frac{\zeta}{|\rho-1|}-\alpha\right)\begin{cases}0 & \rho>1\\ \frac{1}{2} & \rho=1\\ 1 & \rho<1\end{cases} \tag{A.14}$$

$P_{1,0;0}$ occurs in: ${}_K\mathrm{u}_z$, ${}_K\sigma_{rr}$, ${}_K\sigma_{zz}$, ${}_K\sigma_{\theta\theta}$, ${}_z\mathrm{u}^{\mathrm{i}}_z$, ${}_z\phi^i$

$$P_{1,0;0}(\rho,\zeta,\alpha) = -\frac{k\zeta}{2\pi\sqrt{\rho}}\left(\mathbf{K}+\frac{1-\rho}{1+\rho}\mathbf{\Pi}\right) \tag{A.15}$$

$$+\,\mathrm{sign}\left(\arctan\frac{\zeta}{|\rho-1|}-\alpha\right)\begin{cases}1 & \rho<1\\ \frac{1}{2} & \rho=1\\ 0 & \rho>1\end{cases} \tag{A.16}$$

$P_{1,0;1}$ occurs in: ${}_z\mathrm{u}^{\mathrm{i}}_z, {}_z\sigma^{\mathrm{i}}_{zz}, {}_z\sigma^{\mathrm{i}}_{rr}, {}_z\sigma^{\mathrm{i}}_{\theta\theta}$

$$P_{1,0;1}(\rho,\zeta) = \frac{k}{2\pi\sqrt{\rho}}\left(\frac{k^2\left(1-\zeta^2-\rho^2\right)}{4\rho k'^2}\mathbf{E}+\mathbf{K}\right) \tag{A.17}$$

$P_{1,0;2}$ occurs in: ${}_z\sigma^{\mathrm{i}}_{zz}, {}_z\sigma^{\mathrm{i}}_{rr}$

$$P_{1,0;2}(\rho,\zeta) = \frac{k^3\zeta}{8\pi k'^2\rho^{3/2}}\left(\frac{k^4\left(1-\left(\rho^2+\zeta^2\right)^2\right)}{4\rho^2k'^2}\mathbf{E}-\frac{k^2\left(1-\zeta^2-\rho^2\right)}{4\rho k'^2}\mathbf{K}\right) \tag{A.18}$$

$P_{1,1;-1}$ occurs as part of the Lipschitz–Hankel integrals below, in: $P_{2,0;-1}$, $P_{2,1;0}$

$$P_{1,1;-1}(\rho,\zeta,\alpha) = \frac{\zeta}{2\pi\sqrt{\rho}}\left(\frac{2}{k}\mathbf{E}-\left(\frac{k\rho}{2}+\frac{k}{2\rho}+\frac{2-k^2}{k}\right)\mathbf{K}+\frac{k}{2}\frac{(1-\rho)^2}{\rho}\mathbf{\Pi}\right)$$

$$+\frac{1}{2}\mathrm{sign}\left(\arctan\frac{\zeta}{|\rho-1|}-\alpha\right)\begin{cases}\frac{1}{\rho} & \rho>1\\ 1 & \rho=1\\ \rho & \rho<1\end{cases} \tag{A.19}$$

$$\left.\frac{P_{1,1;-1}(\rho,\zeta,\alpha)}{\rho}\right|_{\rho=0} = \frac{1}{2}\left(\mathrm{sign}(\arctan\zeta-\alpha)-\frac{\zeta}{\sqrt{1+\zeta^2}}\right) \tag{A.20}$$

$P_{1,1;0}$ occurs in: ${}_z\mathrm{u}^{\mathrm{i}}_r, {}_z\sigma^{\mathrm{i}}_{rr}, {}_z\sigma^{\mathrm{i}}_{\theta\theta}$, ${}_K\mathrm{u}_r$, ${}_K\sigma_{rr}$, ${}_K\sigma_{rz}$

$$P_{1,1;0}(\rho,\zeta) = \frac{2}{\pi k\sqrt{\rho}}\left(\frac{2-k^2}{2}\mathbf{K}-\mathbf{E}\right) \tag{A.21}$$

$$\left.\frac{P_{1,1;0}(\rho,\zeta)}{\rho}\right|_{\rho=0} = \frac{1}{2}\left(\frac{1}{1+\zeta^2}\right)^{\frac{3}{2}} \tag{A.22}$$

$P_{1,1;1}$ occurs in: ${}_z\mathrm{u}^{\mathrm{i}}_r, {}_z\sigma^{\mathrm{i}}_{rr}, {}_z\sigma^{\mathrm{i}}_{\theta\theta}$, ${}_K\sigma_{\theta\theta}$, ${}_K\sigma_{rz}$

$$P_{1,1;1}(\rho,\zeta) = \frac{k\zeta}{2\pi\sqrt{\rho}}\left(\frac{2-k^2}{2k'^2}\mathbf{E}-\mathbf{K}\right) \tag{A.23}$$

$$\left.\frac{P_{1,1;1}(\rho,\zeta)}{\rho}\right|_{\rho=0} = \frac{3}{2}\zeta\left(\frac{1}{1+\zeta^2}\right)^{\frac{5}{2}} \tag{A.24}$$

$P_{1,1;2}$ occurs in: ${}_z\sigma^{\mathrm{i}}_{rz}$

$$P_{1,1;2}(\rho,\zeta) = \frac{k}{2\pi\rho^{3/2}}\left(\frac{k^2}{4\rho k'^2}\left(\frac{k^2}{k'^2}-1-\rho^2\right)\mathbf{E} + \left(1-\frac{k^2\zeta^2(2-k^2)}{8\rho k'^2}\right)\mathbf{K}\right) \tag{A.25}$$

$$\left.\frac{P_{1,1;2}(\rho,\zeta)}{\rho}\right|_{\rho=0} = \frac{3}{2}(4\zeta^2-1)\left(\frac{1}{1+\zeta^2}\right)^{\frac{7}{2}} \tag{A.26}$$

$P_{2,\nu;\lambda}$ All the following are derived using recurrence formulae as given by Eason et al. (1955), so the explicit expressions, in terms of elliptic integrals, are not given, although they may be obtained from the above formulae.

$P_{2,0;-1}$ occurs in: ${}_r\psi^{\mathrm{i}}$

$$P_{2,0;-1}(\rho,\zeta,\alpha) = -\rho P_{1,1;-1}(\rho,\zeta,\alpha) - \zeta P_{1,0;-1}(\rho,\zeta,\alpha) \tag{A.27}$$

this is discontinuous, so the angle parameter must be carried over to the constituent parts – this similarly applies to some of the following.

$P_{2,0;0}$ occurs in: ${}_ru^{\mathrm{i}}_z$, ${}_r\phi^{\mathrm{i}}$

$$P_{2,0;0}(\rho,\zeta,\alpha) = 2P_{1,0;-1}(\rho,\zeta,\alpha) - P_{0,0;0}(\rho,\zeta) \tag{A.28}$$

$P_{2,0;1}$ occurs in: ${}_ru^{\mathrm{i}}_z, {}_r\sigma^{\mathrm{i}}_{rr}, {}_r\sigma^{\mathrm{i}}_{\theta\theta}$

$$P_{2,0;1}(\rho,\zeta,\alpha) = 2P_{1,0;0}(\rho,\zeta,\alpha) - P_{0,0;1}(\rho,\zeta) \tag{A.29}$$

$P_{2,0;2}$ occurs in: ${}_r\sigma^{\mathrm{i}}_{rr}, {}_r\sigma^{\mathrm{i}}_{zz}$

$$P_{2,0;2}(\rho,\zeta) = 2P_{1,0;1}(\rho,\zeta) - P_{0,0;2}(\rho,\zeta) \tag{A.30}$$

$P_{2,1;0}$ occurs in: ${}_ru^{\mathrm{i}}_r, {}_r\sigma^{\mathrm{i}}_{rr}, {}_r\sigma^{\mathrm{i}}_{\theta\theta}$

$$P_{2,1;0}(\rho,\zeta,\alpha) = 2P_{1,1;-1}(\rho,\zeta,\alpha) - P_{0,1;0}(\rho,\zeta,\alpha) \tag{A.31}$$

$$\left.\frac{P_{2,1;0}(\rho,\zeta,\alpha)}{\rho}\right|_{\rho=0} = \operatorname{sign}(\arctan\zeta-\alpha) - \frac{\zeta(2\zeta^2+3)}{2(\zeta^2+1)^{3/2}} \tag{A.32}$$

$P_{2,1;1}$ occurs in: ${}_ru^{\mathrm{i}}_r, {}_r\sigma^{\mathrm{i}}_{rr}, {}_r\sigma^{\mathrm{i}}_{\theta\theta}, {}_r\sigma^{\mathrm{i}}_{rz}$

$$P_{2,1;1}(\rho,\zeta) = 2P_{1,1;0}(\rho,\zeta) - P_{0,1;1}(\rho,\zeta) \tag{A.33}$$

$$\left.\frac{P_{2,1;1}(\rho,\zeta)}{\rho}\right|_{\rho=0} = \frac{3}{2(\zeta^2+1)^{5/2}} \tag{A.34}$$

$P_{2,1;2}$ occurs in: ${}_r\sigma^{\mathrm{i}}_{rz}$

$$P_{2,1;2}(\rho,\zeta) = 2P_{1,1;1}(\rho,\zeta) - P_{0,1;2}(\rho,\zeta) \tag{A.35}$$

$$\left.\frac{P_{2,1;2}(\rho,\zeta)}{\rho}\right|_{\rho=0} = \frac{15\zeta}{2(\zeta^2+1)^{7/2}} \tag{A.36}$$

Appendix B. Distributed Kelvin solution

An integration of a force density (traction) over a circular region is required. We start with the solution to the Kelvin problem, expressed in terms of the axial component of the vector Papkovich–Neuber potential is

$$\phi = \frac{F}{2\pi(\kappa+1)R} \tag{B.1}$$

where: R is the distance from the point of application, of the force F, which is in the positive z-direction. Using cylindrical coordinates (radial distance, angle, axial distance), consider this to act at a point on a plane with coordinates $(s,\theta,0)$ and the field point is at $(r,0,z)$ then the separation is

$$R = \sqrt{r^2 + s^2 - 2rs\cos\theta + z^2} \tag{B.2}$$

We wish to integrate over the area of the disc $s < a$

$$\phi = \frac{f}{2\pi(\kappa+1)} \int_0^a \int_{-\pi}^{\pi} \frac{s\,\mathrm{d}\theta\,\mathrm{d}s}{\sqrt{r^2 + s^2 - 2rs\cos\theta + z^2}} \tag{B.3}$$

where f is the force density (traction) on the interior surface.

The inner integral is amenable, to give

$$\phi = \frac{f}{2\pi(\kappa+1)} \int_0^a \frac{4s}{\sqrt{(r+s)^2 + z^2}} \mathbf{K}\left(\frac{4rs}{(r+s)^2 + z^2}\right) \mathrm{d}s \tag{B.4}$$

where $\mathbf{K}()$ is the complete Elliptic integral of the first kind. When expressed in terms of the modulus, $k = \sqrt{4rs/((r+s)^2 + z^2)}$ it looks quite simple:

$$\phi = \frac{f}{2\pi(\kappa+1)} \int_0^a 2k\sqrt{\frac{s}{r}} \mathbf{K}(k)\,\mathrm{d}s \tag{B.5}$$

and the integrand can be set as the product of the radial coordinate s and a Lipschitz–Hankel Integral, see Appendix A

$$\phi = \frac{f}{(\kappa+1)} \int_0^a s I_{0,0;0}(s,r,z)\,\mathrm{d}s \tag{B.6}$$

After rearranging a formula given in Eason et al. (1955) for differentiation by a radial component

$$a^{\mu} I_{\mu-1,\nu;\lambda+1} = \frac{\partial}{\partial a} a^{\mu} I_{\mu,\nu;\lambda} \tag{B.7}$$

Using this, with $(\mu,\nu;\lambda)$ as $(1,0;-1)$, and s for a, include the limits and integrate, now, by s

$$\int_0^a s I_{0,0;0}\,\mathrm{d}s = \left[s I_{1,0;-1}\right]_0^a \tag{B.8}$$

Substituting in the limits and substituting the result to Eq. (B.6) gives

$$\phi = \frac{f\ a}{(\kappa+1)} I_{1,0;-1} \tag{B.9}$$

as we require.

References

Barber, J.R., 2002. Elasticity, second ed. Kluwer Academic Publishers, Dordrecht.

Blomerus, P.M., Hills, D.A., 1998. An efficient procedure for modelling limited plastic flow. Proceedings of the Institution of Mechanical Engineers Part C – Journal of Mechanical Engineering Science 212 (8), 731–740.

Christian, J.W., Crocker, A.G., 1980. Dislocations in lattice transformations. In: Nabarro, F.R.N. (Ed.), . In: Dislocations in Solids, vol. 3. North-Holland, Amsterdam, pp. 165–249.

Demir, I., Hirth, J.P., Zbib, H.M., 1992. The Somigliana ring dislocation. Journal of Elasticity 28 (3), 223–246.

Eason, G., Noble, B., Sneddon, I.N., 1955. On certain integrals of Lipschitz–Hankel type involving products of Bessel functions. Philosophical Transactions of The Royal Society of London – Series A 247, 529–551.

Hills, D., Kelly, P., Dai, D.N., Korsunsky, A.M., 1996. Solution of Crack Problems (The Distributed Dislocation Technique). Kluwer Academic Publishers.

Hurtado, J.A., Weertman, J., 1995. Non-redundant dislocation density field of a circular bar deformed in torsion and the stress gradient hardening effect. Physica Status Solidi (a) 149 (1), 173–186.

Kolesnikova, A.I., Romanov, A.E., 2004. Virtual circular dislocation-disclination loop technique in boundary value problems in the theory of defects. Journal of Applied Mechanics-Transactions of the Asme 71 (3), 409–417.

Korsunsky, A.M., 1996a. The Somigliana ring dislocation revisited. 1. Papkovich potential solutions for dislocations in an infinite space. Journal of Elasticity 44 (2), 97–114.

Korsunsky, A.M., 1996b. The Somigliana ring dislocation revisited. 2. solutions for dislocations in a half space and in one of two perfectly bonded dissimilar half spaces. Journal of Elasticity 44 (2), 115–129.

Kroupa, F., 1960. Circular edge dislocation loop. Czechoslovak Journal of Physics 10 (4), 284–293.

Love, A.E.H., 1927. Treatise on the Mathematical Theory of Elasticity, fourth ed. Dover.

Sackfield, A., Barber, J.R., Hills, D.A., Truman, C.E., 2002. A shrink-fit shaft subject to torsion. European Journal of Mechanics A-Solids 21 (1), 73–84.

Salamon, N.J., Comninou, M., 1979. Circular prismatic dislocation loop in an interface. Philosophical Magazine A-Physics of Condensed Matter Structure Defects and Mechanical Properties 39 (5), 685–691.

Salamon, N.J., Dundurs, J., 1971. Elastic fields of a dislocation loop in a two -phase material. Journal of Elasticity 1 (2), 153–164.

Salamon, N.J., Dundurs, J., 1977. Circular glide dislocation loop in a 2-phase material. Journal of Physics C-Solid State Physics 10 (4), 497–507.

Salamon, N.J., Walter, G.G., 1979. Limits of Lipschitz–Hankel integrals. Journal of the Institute of Mathematics and Its Applications 24 (3), 237–254.

Weertman, J., 1996. Dislocation Based Fracture Mechanics. World Scientific Publishing Company.